Evidence for an Explosive Origin of Central Pit Craters on Mars

Nathan R. Williams[1], James F. Bell III[1], Philip R. Christensen[1], Jack D. Farmer[1]

[1]School of Earth and Space Exploration, Arizona State University, Tempe, AZ, USA

Abstract:

Kilometer-scale pit craters are nested in the centers of many impact craters on Mars as well as on icy satellites. They have been inferred to form in the presence of a water-ice rich substrate; however, the process(es) responsible for their formation is still debated. Leading models invoke origins by either explosive excavation, or by subsurface drainage and collapse. If explosive excavation forms central pits, ejecta blankets should be draped around the pits, whereas internal collapse should not deposit significant material outside pit rims. Using visible wavelength images from the MRO CTX and HiRISE instruments and thermal infrared images from the Odyssey THEMIS instrument, we conducted a survey to characterize, in detail, the global population of central pits in impact craters ≥10 km in diameter. We specifically examined the morphology and thermophysical characteristics of the pits for evidence of pit ejecta. Our analysis of thermal images suggests that coarse-grained materials – which we interpret as pit ejecta – are distributed proximally around many central pits on the floors of their parent craters. These observations and interpretations support an explosive origin for central pits on Mars. We present an alternative "uplift contact model" to explain the formation of central pits late in the impact process. Theoretical calculations show that more than enough thermal energy is available via impact melt from the parent crater to form central pits by steam explosions, and such explosions would require only a modest amount (2-6% by volume) of uplifted water-ice. We

therefore propose that central pits on Mars could have formed explosively by the interaction of impact melt and subsurface water-ice.

Introduction:

Nested central pit craters on Mars have remained enigmatic structures for several decades. Their formation is typically believed to be connected with subsurface water due to their relative abundance on Mars and icy satellites, but the exact role of water and the specific process(es) responsible for forming central pits are still debated. In this study, we make thermal inertia observations of central pit craters to test hypotheses for central pit formation. We start with an overview of the previously proposed hypotheses and the gaps in our understanding. Then, we discuss the utility of thermal inertia in remotely determining grain size distributions around central pits. We hypothesize that central pits are formed by explosive excavation or devolatilization during or after impact. After analyzing our results, we present an alternative model for central pit formation that -- uniquely among other pit origin hypotheses -- creates an explosion late enough in the impact process for central pits to be preserved. Finally, we apply our integrated observations to interpret the morphology and thermal properties of central pits in the context of central uplifts and propose testable predictions for the model.

Background:

Central pits occur in many impact structures on Mars and exhibit a crater-in-crater configuration [*e.g.*: Smith, 1976; Hodges, 1978; Barlow *et al*., 2000; Barlow, 2010] (Fig. 1). Kilometer-scale central pits have been identified on the floors or on top of the central peaks of over 1,000 Martian impact craters with diameters as large as 125 km in diameter and down to as small as 5 km in diameter [Smith, 1976; Barlow and Bradley, 1990; Barlow *et al*., 2000; Barlow, 2011]. In our study, we focus on "floor pits" that are deeper than the surrounding floor of their parent craters, as opposed to "summit pits" that occur atop the central peaks. Based an ongoing survey by Barlow [2010, 2011] and this study, central floor pits have a median diameter of 0.16-0.175 parent crater radii, such that a 50 km diameter crater might have a central pit ~8 km wide. Their depths range from very shallow to over 1.5 km below the surrounding impact crater floor.

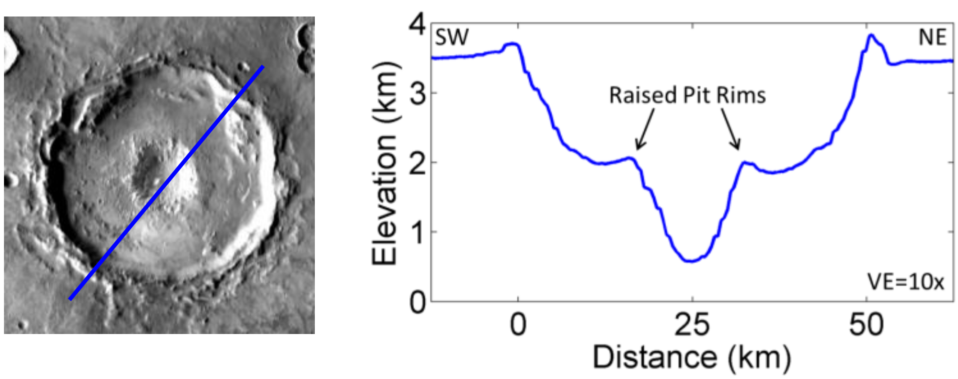

Fig. 1: THEMIS daytime IR mosaic of a 50 km diameter unnamed Martian impact crater containing a central pit at 296.4°E, 17.6°S. A MOLA topographic profile across the center shows typical pit morphology.

Central pit craters on Mars are confined to low and mid-latitudes, within ±70° of the Martian equator [Hodges *et al*., 1980; Barlow, 2011; Garner and Barlow, 2012]. Central pits are also common for impact craters on icy satellites, including Ganymede and Callisto [Smith *et al*., 1979]. Central pits are seldom observed on rocky planets other than Mars, although a few dozen are present on Mercury [Schultz, 1988; Xiao and Komatsu, 2013] and the Moon [Croft, 1981; Schultz, 1976a, 1976b, 1988; Xiao *et al*., 2014].

The presence of water-ice is believed to be involved in typical pit formation [Hodges *et al*., 1980; Croft, 1981]. Although water-ice is not stable on low-latitude Martian surfaces today [Clifford and Hillel, 1983; Mellon *et al*., 1997; Head *et al*., 2003], water was (and might still be) present within the upper few kilometers of the surface even at low latitudes earlier in Mars' history. The possibility of significant subsurface water in pre-impact terrains is supported by the presence of layered ejecta surrounding many fresh Martian impact craters [Carr *et al*., 1977; Gault and Greeley, 1978; Wohletz and Sheridan, 1983; Barlow *et al*., 2000; Baloga *et al*., 2005] and Mars Odyssey Gamma Ray Spectrometer spectra [Boynton *et al*., 2007]. However, the process(es) responsible for forming central pits in impact craters and the role of water are still debated, and several mechanisms for pit formation have previously been proposed.

Wood *et al*. [1978] proposed explosive decompression may volatilize a subsurface water-rich layer, causing steam explosions and removing the core of central peaks. However, this model suffers from the difficulty of keeping water vapor from escaping early in the impact process before a central pit can be preserved [Croft, 1981; Pierazzo *et al.*, 2005; Senft and Stewart, 2011; Elder *et al*., 2012].

Croft [1981], Bray [2009], Senft and Stewart [2011], Alzate and Barlow [2011] and Elder *et al*. [2012] proposed central pits could form by the melting then gravitational drainage of target water-ice through fractures underlying central uplifts. However, raised rims are also associated with many Martian central pits [Wood *et al.*, 1978; Garner and Barlow, 2012] and would not be expected with collapse structures. These models also require large volumes of water to be drained, which is unrealistic for forming the central pits on the Moon and Mercury.

Passey and Shoemaker [1982], Bray *et al*. [2012], and Greeley *et al*. [1982] proposed central peaks of impacts in weak target materials may collapse to form central pits. However, the abundance of impact craters with central peaks and summit pits in the same regions as impact craters with floor pits suggests the target material should be strong enough to prevent collapse [Barlow, 2011].

Greeley *et al*. [1982] proposed and demonstrated in laboratory experiments that small-scale central pits can be excavated from impacts into layered targets causing central peak detachment. Schultz [1988] also proposed central pits are excavated as a primary result of impacts with low-velocity bolides. However, scaling up to planetary impact craters with diameters of tens of kilometers is problematic because the material-strength crater is larger than the gravity-controlled transient crater, greatly reducing the influence of any strength differences on the final crater morphology [Croft, 1981].

For this study, we group the previously proposed mechanisms for pit formation into those that explosively remove material upward and outward [*e.g*.: Wood *et al*., 1978; Greeley *et al*., 1982; Schultz, 1988] and those that remove material downward [*e.g*.: Croft, 1981; Passey and Shoemaker, 1982]. During a crater-forming explosion, rocks and boulders are ejected out of the crater, layers are proximally uplifted and overturned, and ejecta is draped over the surrounding surface to create raised rims [*e.g.* Melosh, 1989]. The average grain size for ejecta decreases with radial distance from the crater, such that the largest clasts or blocks are proximal to the crater rim [*e.g*.: Gault *et al*., 1963; O'Keefe and Ahrens, 1985; Melosh, 1989; Buhl, 2014]. Features such as sinkholes, which are typical of karst landscapes, and lava tube skylights form by gravitational collapse and do not create raised rims nor emplace material atop their rims [*e.g.*, Okubo and Martel, 1998; Salvati and Sasowsky, 2002; Cushing *et al*., 2007; Robinson *et al*., 2012]. The presence or absence of an ejecta blanket around central pits provides one way to distinguish between explosive versus collapse scenarios for the formation of central pits. A property of ejecta blankets is decreasing average grain size with distance from an explosively-derived crater.

Data and Methods:

For this study, we surveyed and identified impact craters > ~10 km in diameter containing central floor pits within ±60° latitude of the Martian equator using the Java-based planetary geographic information system program JMARS [Christensen *et al*., 2009]. Central pits were identified as distinctive circular depressions in the center of an impact crater that appeared to be deeper than the parent crater floor based on the available imaging and topography. Many small impact craters with diameters <10 km containing central depressions were excluded from our survey due to poor spatial resolution, as well as craters we could not confidently determine had depressions deeper than the parent floor. We excluded summit pits that occur atop central peaks and are not deeper than the parent crater floor to avoid potential bias from coherent rock or boulders on the sides of the central peaks. We also excluded ambiguous structures that might be peak rings or concentric terraces, especially in craters near the Martian simple to complex crater transition of ~6-7 km diameter [Garvin *et al*., 2000, 2003].

Diameters were measured for both the central pits and their parent craters. Most central pits were too small to identify in the 128 pixel/deg (460 m/px) Mars Orbiter Laser Altimeter (MOLA) global mosaic [Smith *et al*., 2001], so the ~100 m/pixel Mars Odyssey mission Thermal Emission Imaging Spectrometer (THEMIS) [Christensen *et al*., 2004] calibrated daytime infrared (IR) global mosaic [Edwards *et al*., 2011] was used instead, which provides nearly complete coverage to ±60° latitude. THEMIS daytime IR images show topography as shaded relief, since sun-facing slopes are typically warmest. Higher resolution visible images were also used to observe finer-scale morphology and distinguish central morphologies that appeared ambiguous in THEMIS daytime IR. Primarily, we used Mars Reconnaissance Orbiter mission Context Camera (CTX) [Malin *et al*., 2007; Bell *et al*., 2013] images at ~ 6 m/pixel that were map-projected and photometrically stretched from Planetary Data System (PDS) raw electronic data records, and where available we used High Resolution Imaging Science Experiment (HiRISE) [McEwen *et al*., 2007] images at ~ 0.25 to 1.3 m/pixel that were map-projected and photometrically stretched from PDS calibrated reduced data records. The global dust environment for central pit crater context is shown using Thermal Emission Spectrometer (TES) solar energy reflectivity (albedo) integrated from 0.3 to 2.9 µm [Christensen *et al*., 2001].

During the formation of impact and other explosive craters, coarse debris are typically ejected and scattered outside the crater. Large blocks and coarse grains have a higher thermal inertia than finer-grained materials and hold on to their heat longer through the night. This thermal inertia can be calculated from nighttime thermal images and used to estimate average grain size [Christensen, 1986]. We therefore used the THEMIS thermal inertia global mosaic as a quantitative proxy for average grain size, such that coarse-grained or blocky materials have relatively higher thermal inertias (warmer at night) while dust, sand, and other fine-grained materials have lower thermal inertias (cooler at night) [Christensen, 1986; Fergason *et al*., 2006; Edwards *et al*., 2009; Edwards *et al*., 2011]. THEMIS nighttime images and thermal inertias have previously been used to identify blocky ejecta rays from impact craters on Mars that otherwise show little or no albedo variation in visible images but where grain size trends are seen with respect to distance from the crater [McEwen *et al*., 2005; Tornabene *et al*., 2006]. Central pits with an annulus or a geographically skewed patch of higher thermal inertia material nearer the pit rim than more distally across the surrounding parent crater floor may be classified as having a fining average grain size with radial distance, consistent with ejecta.

To measure the trend of thermal inertias, we circumferentially averaged the THEMIS thermal inertia mosaic over central pit craters in intervals of 0.1 parent crater radii. Because most central pits are <0.2 crater radii, we compare pit-proximal averaged thermal inertia values within the interval from 0.2-0.3 crater radii versus more distal averaged thermal inertia values at 0.5-0.6 crater radii. A Student's t-test is then performed on the differences between proximal and distal averaged thermal inertias for the population of central pits. A significance level of $P \geq 0.05$ would be deemed not statistically significant and serves as our null hypothesis: thermal inertia and average grain size do not decrease radially away from pit rims. For $P<0.05$, a radial decrease in thermal inertia with distance from the pit rim would be deemed statistically significant and we would reject the null hypothesis and support an alternative hypothesis that ejecta surrounds central pits.

Results:

We identified central floor pits within 654 parent craters ~10 km diameter or larger between ±60° latitude of the Martian equator (Fig. 2). Additional smaller craters with central pits exist [Barlow, 2010, 2011], but are not well-resolved in the THEMIS thermal images used for this study. MOLA topographic profiles have very coarse resolution and may only provide insight to the largest central pit craters (Fig. 1), although complete and partially rimmed pits frequently occur in the highlands terrains [Garner and Barlow, 2012]. We identified central pits in parent impact craters with diameters ranging from ~8 to 114 km, with 95% of those parent craters being <50 km in diameter and excluding smaller potential central pit craters. The surveyed central pits have a median diameter ratio to their parent craters of 0.175 with a standard deviation of 0.037 (Fig. 3). These results are comparable to the median ratio of 0.16 found by Barlow [2011].

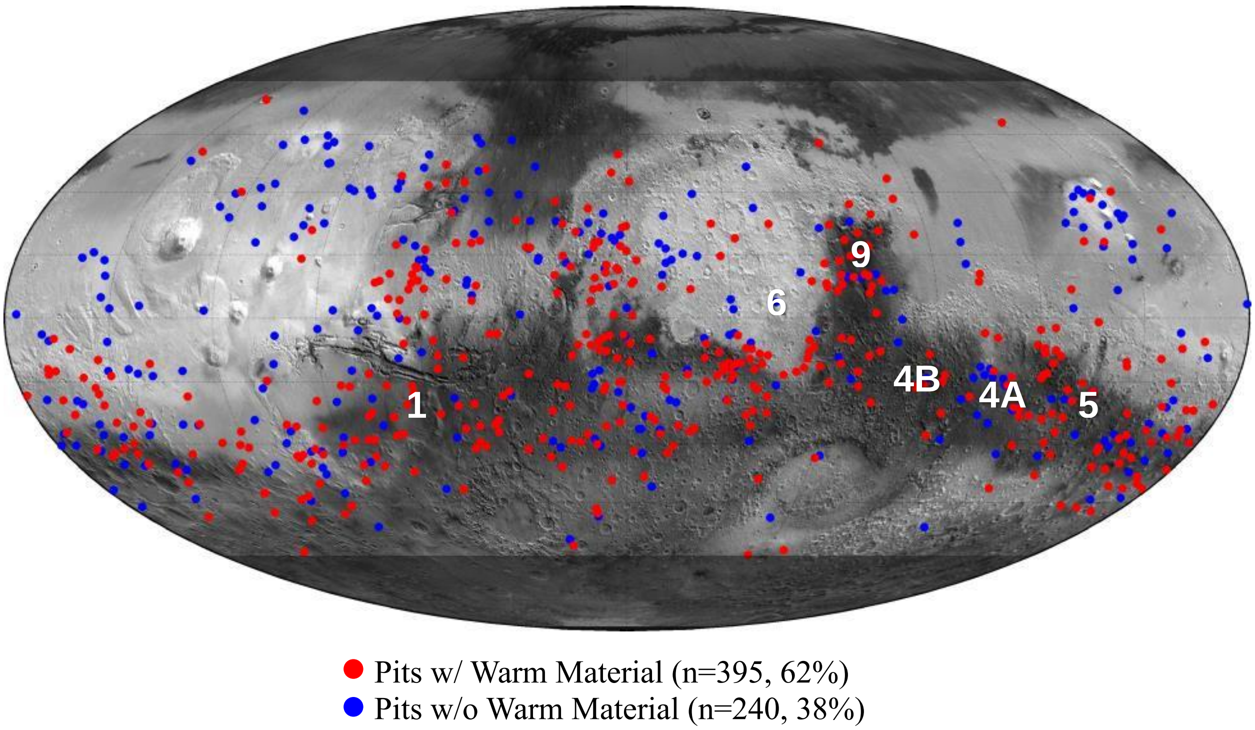

Fig. 2: Distribution of 654 central pit craters identified in our survey of the THEMIS daytime global mosaic, within ±60° degrees of the Martian equator, overlain on the TES albedo basemap [Christensen *et al*., 2001] and presented in a Mollweide equal area projection. Locations of Figs. 1, 4A, 4B, 5, 6, and 9 are highlighted.

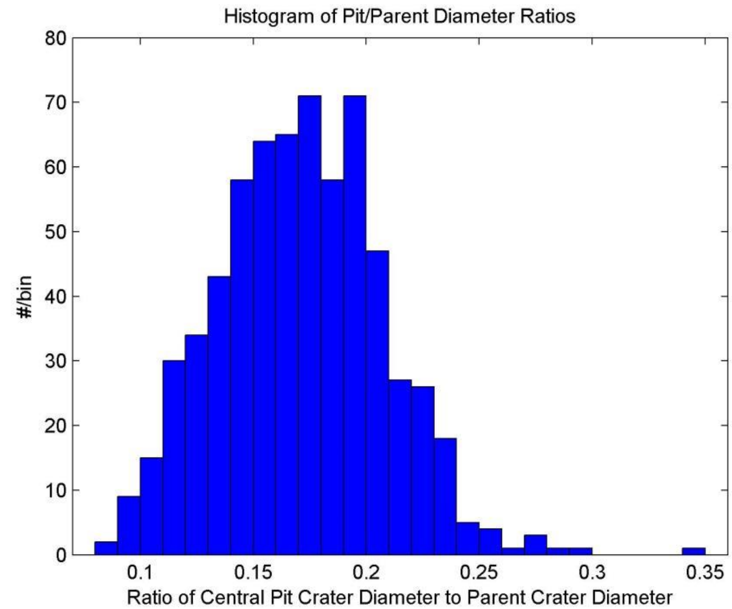

Fig. 3: Histogram showing the range of diameter ratios between central pits and their parent craters that we measured. The median value is 0.175 with a standard deviation of 0.037.

Based on THEMIS-derived thermal inertias, most central pits showed higher thermal inertia (coarser) material near their rim than more distally on the parent crater floor (*e.g.* Fig. 4). 635 of the 654 central pits had thermal images over their parent crater floors, of which 395 (62%) had higher average proximal thermal inertias outside the pits (between 0.2-0.3 crater radii) than more distally (between 0.5-0.6 crater radii), and 240 (38%) had the same or lower thermal inertia proximally than distally. Notably, 76% (254 out of 333) of central pits with diameters >20 km have radially decreasing thermal inertia trends, 80% (175 out of 216) of central pits with near-pit thermal inertia values >300 TIU (less dusty) have radially decreasing thermal inertia trends, and 89% (74 out of 83) of central pits satisfying both of the above selection criteria have radially decreasing thermal inertia trends. Pits with proximal high and radially decreasing thermal inertias in THEMIS images sometimes show large blocky debris (up to tens of meters wide) in visible CTX and HiRISE images (Fig. 5), while pits that did not show proximally high nor decreasing thermal inertias typically appeared blanketed or mantled (Fig. 6).

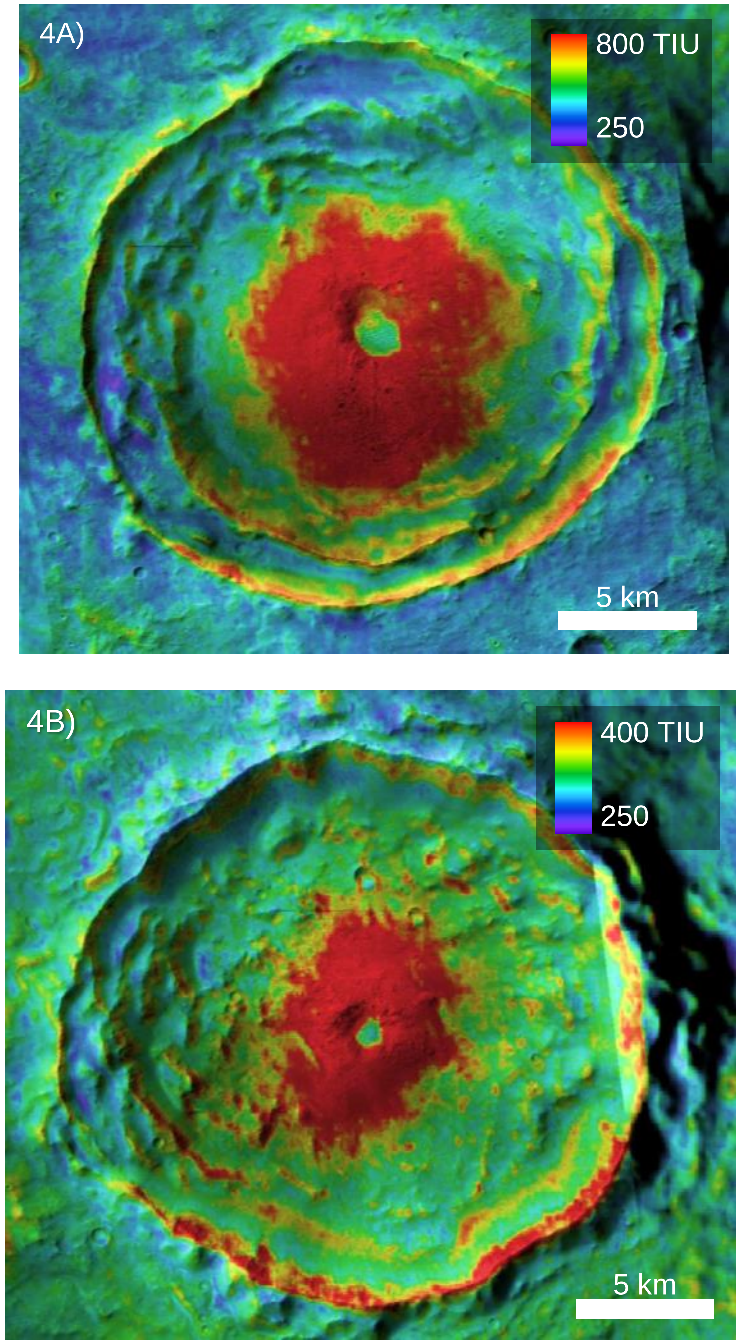

Fig. 4: THEMIS nighttime (color) and CTX visible (shading) images showing radially decreasing high thermal inertia material interpreted as ejecta surrounding two central pit craters at A) 18.4°S, 102.7°E, and B) 14.9°S, 93.2°E. Color scales indicate thermal inertia values.

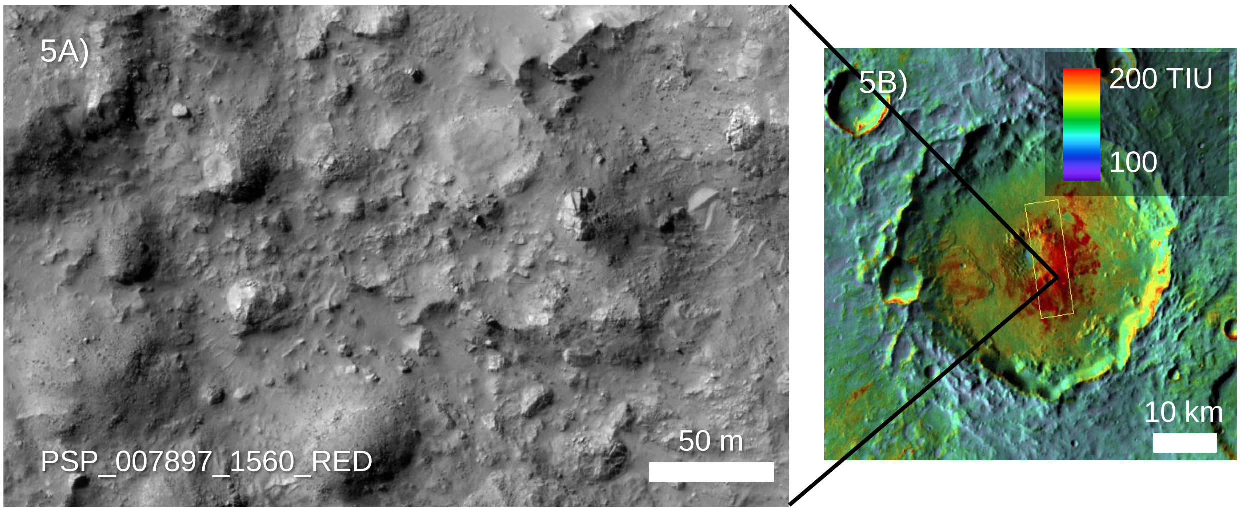

Fig. 5: A) HiRISE image showing large blocks near a central pit crater at 23.8°S, 126.8°E. B) THEMIS nighttime IR (color) over daytime IR (shading) context image showing high-thermal inertia material inferred as being blocky and confirmed by the HiRISE image. Black lines indicate location of A. Yellow box in B indicates footprint of HiRISE image.

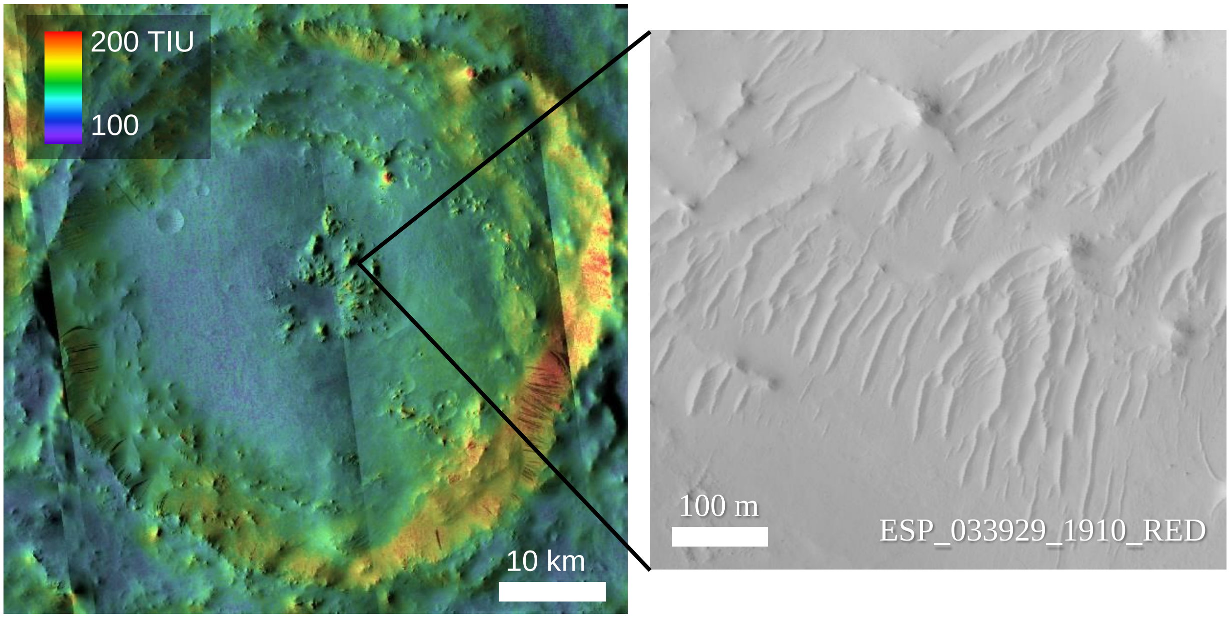

Fig. 6: A) THEMIS nighttime IR (color) over CTX visible (shading) image showing a central pit crater at 10.9°N, 50.8°E without a radially decreasing thermal inertia. Average thermal inertia values are uniformly low across the crater floor and associated with a coating of fine-grained dust. B) HiRISE visible image enlargement of an area near the central pit showing low-contrast dust mantling the terrain.

We conducted a paired Student's t-test to determine the confidence interval of the measured thermal inertia decreases from 0.2-0.3 crater radii to 0.5-0.6 crater radii. For the 635 central pit craters with thermal images, the t-test returns a $P<0.01$ indicating extreme statistical significance. We therefore reject our null hypothesis that thermal inertia and average grain size do not decrease radially away from pit rims, and support an alternative hypothesis that pits are surrounded by ejecta with grain size decreasing with distance away from the pit.

Central pits in Tharsis, Elysium, Arabia, and other dusty regions, characterized by high TES albedos and low thermal inertia values, tend to not be surrounded by material with radially decreasing thermal inertia trends (Fig. 1). The median proximal thermal inertia for central pits with radially decreasing thermal inertias is 283 thermal inertia units (1 TIU = 1 J $m^{-2}K^{-1}s^{-1/2}$) with a standard deviation of 121 TIU, while the median proximal thermal inertia for central pits with other, radially non-decreasing thermal inertia trends is 205 TIU with a standard deviation of 145 TIU (Fig. 7).

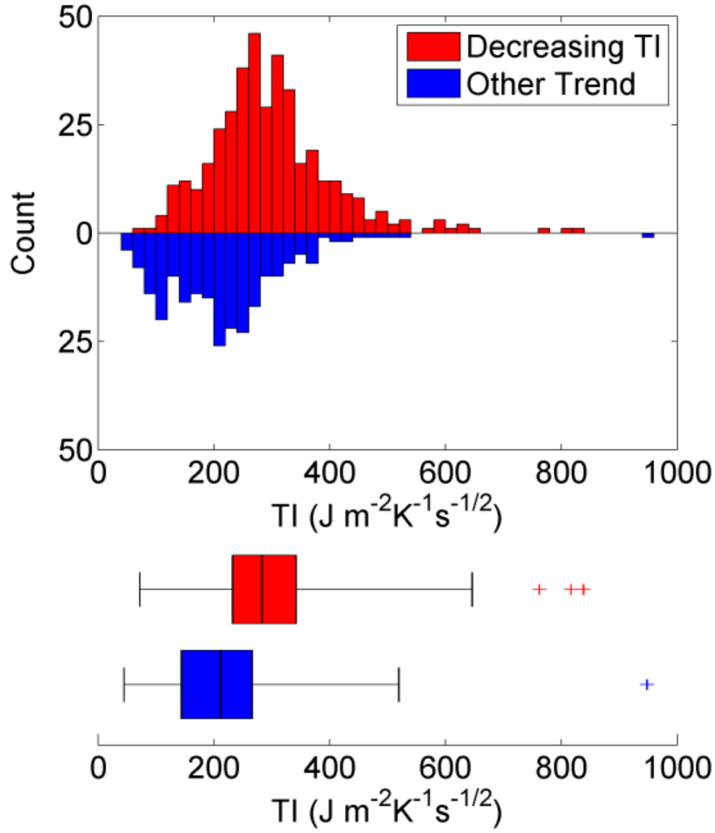

Fig. 7: Histogram and box-and-whisker plot of central pit craters exhibiting radially decreasing thermal inertia trends (red) and radially non-decreasing thermal inertia trends (blue) plotted against THEMIS thermal inertia values. Lower thermal inertias are indicative of finer average grain size and dustiness.

Smaller central pits also tend not to show radially decreasing thermal inertias (Fig. 8). Based on the population of impact craters observed with THEMIS data, the median diameter for parent craters containing pits with warm material is ~23.3 km and the median diameter for craters with pits lacking it is ~16.7 km, both cases being above the simple/complex transition of 6-7 km for Martian craters [Garvin *et al*., 2000, 2003].

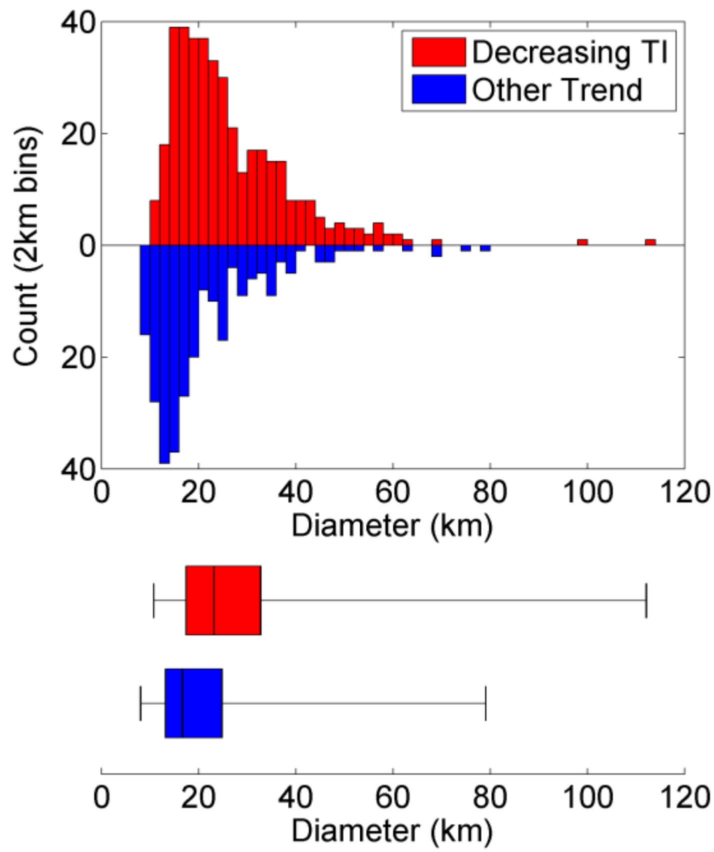

Fig. 8: Histogram and box-and-whisker plot of craters containing central pits exhibiting radially decreasing thermal inertia trends (red) and radially non-decreasing thermal inertia trends (blue) plotted against parent crater diameter.

Discussion:

The raised rims around some pits [Wood, 1978; Garner and Barlow, 2012] are suggestive of explosive excavation, similar to their parent craters, which also have raised rims. As discussed by Garner and Barlow [2012], raised rims are more frequently observed in larger central pits than smaller ones. They also argue that the preferred distribution of rimmed pits in highlands regions and non-rimmed pits in volcanic plains suggests that target material strength and/or volatile content may also limit the expression of raised rims. Some very small scale pits on Mars believed to have formed from volatile release in impact melt have been identified and also exhibit slightly raised rims, although they are not exclusive to crater centers and do not exhibit well-defined ejecta blankets [Tornabene *et al*., 2012; Boyce *et al*., 2012]. Surfaces visible in some CTX and HiRISE images show large (meter-scale) blocks in warm patches adjacent to central pits (*e.g.,* Fig. 5), consistent with the expected correlation between warm material and coarse surfaces. Such blocks and megablocks are commonly observed near explosively-formed craters, including at the Ries crater in Germany [*e.g*. Gault *et al*., 1963], as well as at some Martian craters [*e.g.,* Caudill *et al*., 2012]. Combined with the spatial correlation of warm material and central pits, we interpret the blocks scattered around central pits to be explosively-emplaced pit ejecta.

The observability of high thermal inertia, coarse-grained material appears linked to the size of the pit. Small craters excavate smaller volumes of material that is finer-grained on average than larger craters [*e.g*.: Gault *et al*., 1963; O'Keefe and Ahrens, 1985; Melosh, 1989; Buhl, 2014]. Fine-grained rocks are more easily eroded or buried than coarser-grained rocks, so the coarser ejecta at larger pits should be preferentially preserved and less buried. Surface diurnal thermal inertias are sensitive to materials within a few thermal skin depths (several centimeters) of the surface, so any ejecta would have to be buried by no more than a few centimeters of dust in order to be observable. Accumulated dust and sand is frequently observed on Mars and is indicated in our analysis as low thermal inertia values due to dust's fine grain size (Fig. 6). The smaller grain size distribution of ejecta for smaller craters is therefore expected to decrease the positive detection of ejecta using diurnal thermal inertias.

The presence of high thermal inertia material on parent crater floors near pits would not necessarily need to be due to ejecta. To avoid many false-positives, we have calculated the trend in thermal inertia (grain size) with radial distance from the pit. For example, post-impact lava or perhaps impact melt flows occur on the floors of some craters containing central and have high thermal inertias, although small flow lobes are easily distinguishable (Fig. 9), and more extensive lava or impact melt flows could potentially fill central pits. We expect impact melt ponds to be distributed throughout the crater floor, so measuring a radially decreasing trend in thermal inertia as opposed to only using high thermal inertia values avoids this problem in most cases. Patchy or partial erosional uncovering of consolidated parent crater fill rocks could also explain higher thermal inertias relative to the surrounding crater floor; however, we consider the selective removal of significant amounts of dust from the centers of parent craters, but not in the dusty plains surrounding many parent craters, to be unlikely. Additionally, significant erosion on the parent crater floor is inconsistent with the presence and preservation of raised rims around many central pits. Thermal inertias are also low for relatively fine-grained aeolian dunes or other bedforms that often form in the centers of craters, and confirmed in CTX and HiRISE images (Fig. 6).

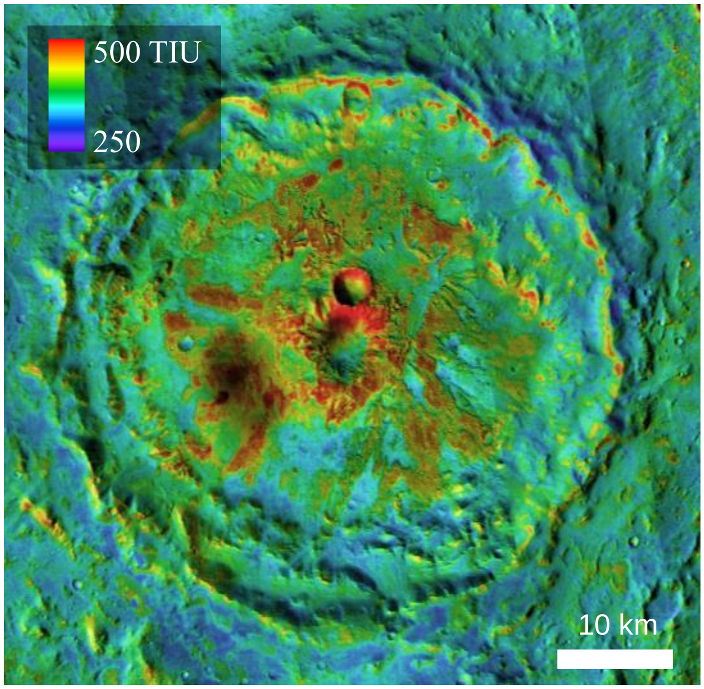

Fig. 9: THEMIS nighttime IR (color) over CTX visible (shading) image showing high thermal inertia lava flow lobes (red, oranges, and yellow irregular bands on crater floor) on the floor of an impact crater containing a central pit at 28.5°N, 83.4°E.

The results of our thermal inertia study are consistent with and support both the Wood *et al*. [1978] and Greeley *et al.* [1982] models; however, each suffers from a critical weakness. The Wood *et al*. [1978] model for an explosive pit origin suffers from the difficulty of keeping vapor from escaping early in the impact process before a pit can be preserved. The Greeley *et al*. [1982] central peak detachment model also suffers from issues scaling up from the laboratory to planetary impact craters. Alternatively, an explosive reaction could potentially result from mixing of water-ice and molten rock through several mechanisms. For example, a post-impact magmatic intrusion could intrude into a crater and react with the ground water as a maar volcano [Wohletz, 1986; Begét *et al*., 1996]; however, we would not expect such a scenario to consistently form pits in crater centers. Heavy fracturing and brecciation during the impact process may allow fluids (either impact melt, or liquid water) to mobilize and permeate the substrate and come into contact with each other, similar to the fluid flow described by Elder *et al*. [2012]. Although liquid water may move freely through fractures, Elder *et al*. finds that impact melt would cool too quickly due to its high melting temperature and larger temperature difference with the country rock. Rain or ice-bearing fallback ejecta could also be deposited on top of impact melt pools or suevite deposits [Segura *et al*., 2002], but that would not necessarily require that pits always form in the centers of their parent craters, nor that they be consistently sized. Below, we describe an alternate model for bringing water into contact with impact melt.

Alternate Pit Formation Model:

We present an alternate hypothesis that -- unique among other pit origin hypotheses -- predicts an explosion late enough in the impact process for central pits to be preserved and has a properly scaled analog. In our uplift contact model, impact central uplifts bring water (as liquid, ice, or both) vertically up and into contact with near-surface impact melt to initiate late-stage steam explosions and form central pits (Fig. 10). Central uplift occurs late in the impact process during the modification stage, after most crater fill has settled [*e.g.*, Melosh, 1989]; thus, pit formation concurrent with central uplift is consistent with the apparent lack of infilling of deep pits. As we describe in the next paragraph, our explosive central pit model is akin to an inverted maar volcano [*e.g.* White and Ross, 2011], except instead of magma rising up into contact with groundwater or permafrost, a water-bearing substrate is uplifted into contact with impact melt. Similarly-scaled events have been observed at monogenetic maar volcanoes with diameters of up to 8 km on the Seward Peninsula in Alaska [Begét *et al*., 1996], where the permafrost buffers the water-magma interaction to achieve high heat transfer efficiencies [Wohletz, 1986].

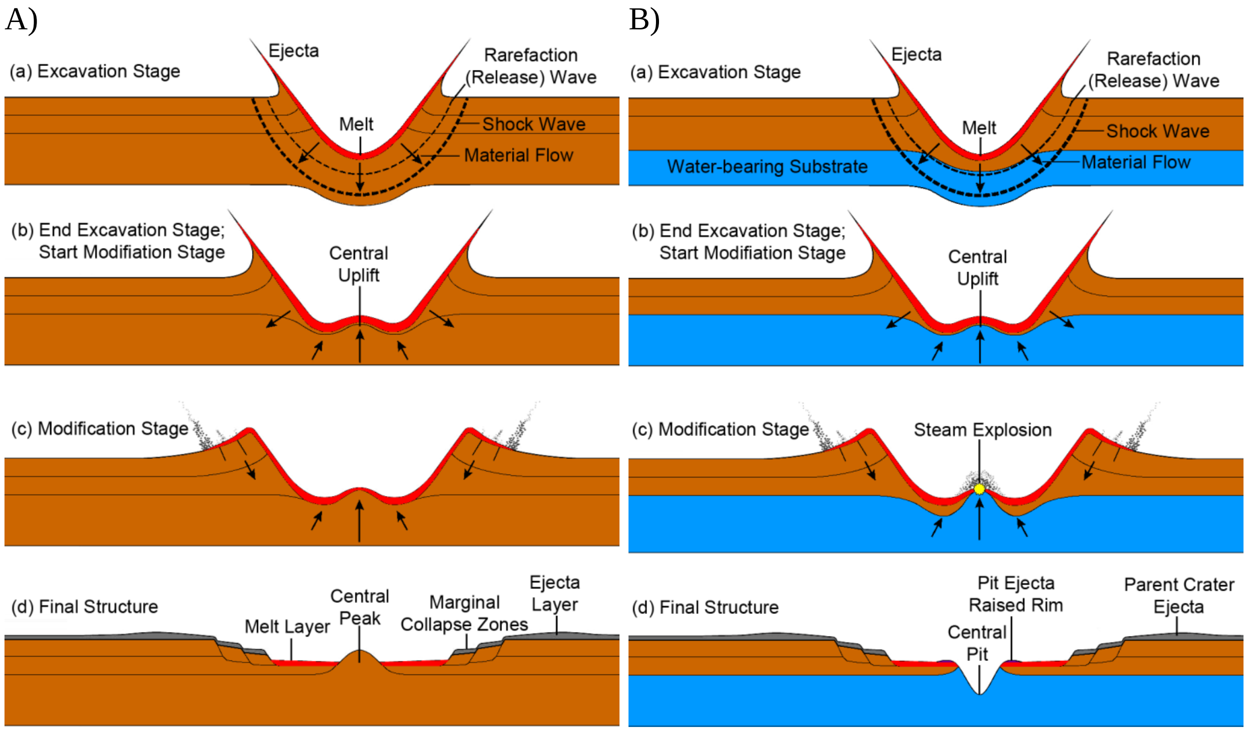

Fig. 10: Schematic cartoons illustrating steps in complex crater formation resulting in: A) a classical central peak [modified from French, 1998], and B) our proposed new "uplift contact model" for Martian central pit crater formation.

As the central uplift rises, it brings deeply-sourced water-bearing rock from below the transient cavity up into contact with shallow crater fill deposits and impact melts. We would not expect significant vertical mixing of sub-transient cavity material outside the central uplift, so these large pits should always be in the centers of their parent impact craters. As the water-bearing central uplift rises into contact with impact melt and other hot debris, the thermal energy from the melt may be transferred to the water, resulting in a steam explosion to eject material outward, raise rims, and deposit ejecta surrounding the pits (with average grain sizes decreasing with radial distance, as we found in this study). As material is ejected outwards, the walls may become unstable and slump hot debris and impact melt into the pit cavity. There, the new rush of melt and hot rocks may again react with uplifting water to recharge the system and iteratively trigger a series of explosions to further deepen and widen the central pit. When central uplift slows, the vertical mixing of water decreases and the explosions will cease.

We explored the theoretical plausibility of whether enough thermal energy could have been available in a post-impact environment to initiate steam explosions capable of creating kilometer-scale central pits. We started with the empirical model shown below which predicts the mass ratio of melted (m_m) to displaced (m_d) impact target materials in a silicate target (Eq. 1) [O'Keefe and Ahrens, 1982; Melosh, 1989]:

$$m_m/m_d=1.6\times10^{-7}\times(g\times D_i)^{0.83}\times v_i^{0.33} \quad (1),$$

where g is planetary gravity, D_i is parent crater diameter and v_i is bolide velocity. We assign the following values for our calculations: gravity g = 3.711 m/s^2 and bolide velocity v_i = 10 km/s [Ivanov *et al.*, 2002]. We also assumed that any melt generated remained within the parent crater. Finally, we modeled the parent crater as a half-ellipsoid and applied the mass fraction to determine the volume and mass of melt produced (Eqs. 2,3):

$$V_m=(m_m/m_d)\times(2/3)\times\pi\times d_i\times(D_i/2)^2 \quad \text{(2) and}$$

$$m_m=\rho_m/V_m \quad (3),$$

where V_m is the volume of melt, d_i is the depth of the parent crater, and ρ_m is the density of the melt. We assume a depth of complex craters (in km) of d_i = 0.357$D_i^{0.52}$ [Tornabene *et al.*, 2013]. Sato and Taniguchi [1997] used the following empirical equation to predict the energy required to form a crater via volcanic, nuclear, and chemical explosions, independent of origin. The equation can similarly be applied to central pits (Eq. 4):

$$E_c=4.45\times10^6\times D_p^{3.05} \quad (4),$$

where E_c is the energy of pit formation and D_p is the diameter of the pit, for which we assume a median pit-to-parent crater diameter ratio of 0.16 [Barlow, 2010, 2011]. The total thermal energy transfer required to melt ice and boil water to steam can be calculated using specific and latent heats (Eq. 5):

$$H_w=m_w\times L_f+m_w\times c_{lq}\times\Delta T_w+m_w\times L_v \quad (5),$$

where H_w is the energy transferred to the water, m_w is the mass of water, L_f is the latent heat of fusion, c_{lq} is the specific heat of liquid water, ΔT_w is the temperature change of liquid water, and L_v is the latent heat of vaporization. We assign values for L_f = 3.34x10^5 J/kg, c_{lq} = 4.187 x10^3 J/kg·K, and L_v = 2.257 x10^6 J/kg [Moran and Shapiro, 2008]. Evaluating Eq. 5, we see that an investment of 3.023x10^6 J is required to turn 1 kg of water from ice (273 K) to steam (373 K). We assume that the steam is not heated to higher temperatures, although a smaller amount of superheated steam might also satisfy the energy requirements for explosivity. The thermal energy of vaporization, specifically the step of converting water to steam, can be transformed to kinetic energy that can form a pit. The mass of steam required is calculated by dividing the pit formation energy from Eq. 4 by the latent heat of vaporization. Dividing this result by the density of ice provides the volume of ice required to form a central pit. As shown in Fig. 11, assuming a half-ellipsoidal pit geometry with the pit depth (in km) $d_p = 0.276D_p^{0.68}$ [Tornabene *et al.*, 2013], only a small amount of water (comprising 2-6% of a central pit's volume) would need to be vaporized to form a central pit for the parent crater diameters observed (5-125 km [Barlow, 2011]).

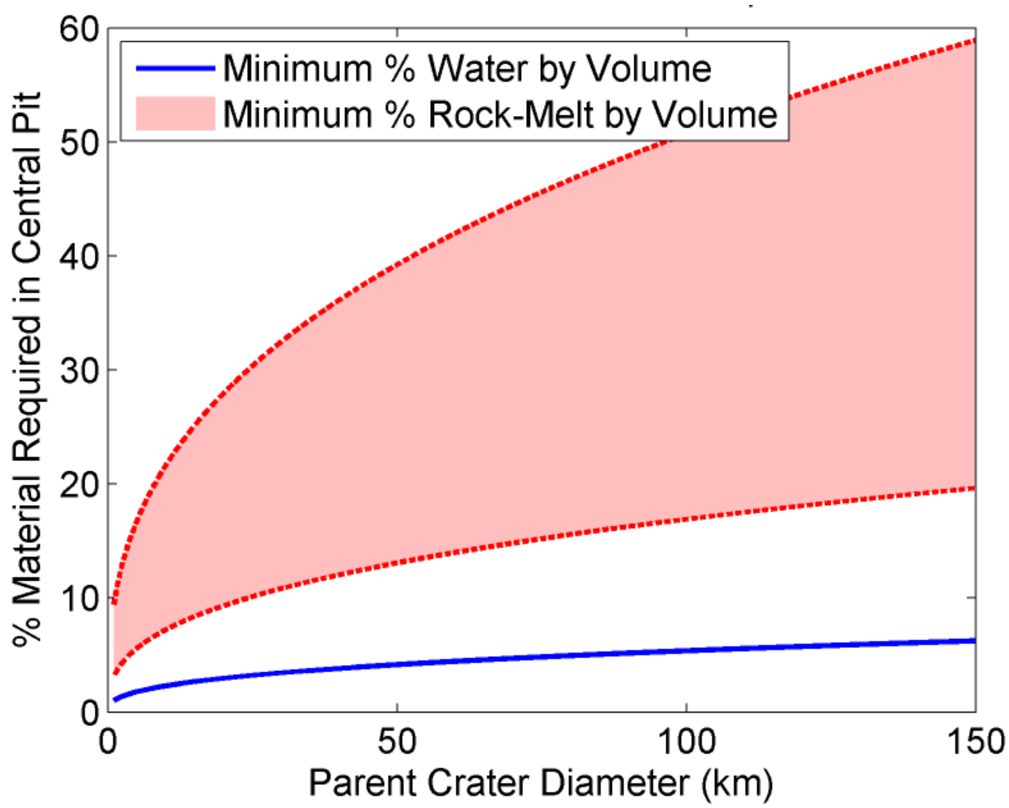

Fig. 11: Required amounts of water and impact melt for heat energy transfer to form a kilometer-scale (pit) crater shown as percent by volume with respect to the volume of a central pit crater. The range in impact melt volume represents uncertainty due to varying heat transfer efficiency between 0.1-0.3.

The amount of thermal energy available in impact melt may also be calculated using specific heats (Eq. 6):

$$E_m = m_m \times c_{pm} \times \Delta T_m = \rho_m \times V_m \times c_{pm} \times \Delta T_m \quad (6),$$

where E_m is the energy required for cooling rock, c_{pm} is the specific heat of rock, ΔT_m is the temperature change of the rock. We assume a basaltic melt composition and assign values of ρ_m = 2900 kg/m^3 [Judd and Shakoor, 1989]; c_{pm} = 1000 J/kg·K [Wohletz, 1986]; and change of temperature (from the basalt solidus to the STP boiling point of water) ΔT_m = 1473 K – 373 K =

1100 K [Wohletz, 1986]. It should be noted that impact melts can also be superheated, perhaps up to 1700°C (1973 K) [Zieg and Marsh, 2005], so our calculations may underestimate the thermal energy available by ~50%. Adiabatic heat transfer efficiency is typically ~0.1 or less due to poor mixing; however, it can reach an optimal efficiency of ~0.3 for water/melt ratios of 0.3-0.5 [Wohletz, 1986]. Such optimal efficiencies are believed to be present for maars in permafrost, as suggested by the largest, kilometer-scale terrestrial maars found in the Seward Peninsula, Alaska [Begét *et al.*, 1996]. Our calculations consider cases with both 0.1 (suboptimal) and 0.3 (optimal) efficiencies.

The mass of impact melt required to vaporize ice to steam can be calculated by setting the total heat transfer H_w from Eq. 5 equal to the product of the heat transfer efficiency and the impact melt thermal energy from Eq. 6. As shown in Fig. 11, the impact melt must comprise a volume greater than or equal to 6-18% of the central pit's volume for an optimal thermal efficiency of 0.3, or 17-55% of the central pit's volume for a suboptimal thermal efficiency of 0.1. The total energy transfer required for vaporizing ice (H_w) from Eq. 5 can also be compared to the total energy available from impact melt by multiplying Eq. 6 with the value(s) for heat transfer efficiency (Figs. 12,13). Based on these calculations, sufficient thermal energy should be available via impact melt to vaporize small amounts of ice that act explosively to form central pits within kilometer-scale impact structures. However, not all Martian craters exhibit central pits. Below, we discuss the material requirements may inhibit the explosive formation of some central pits on Mars.

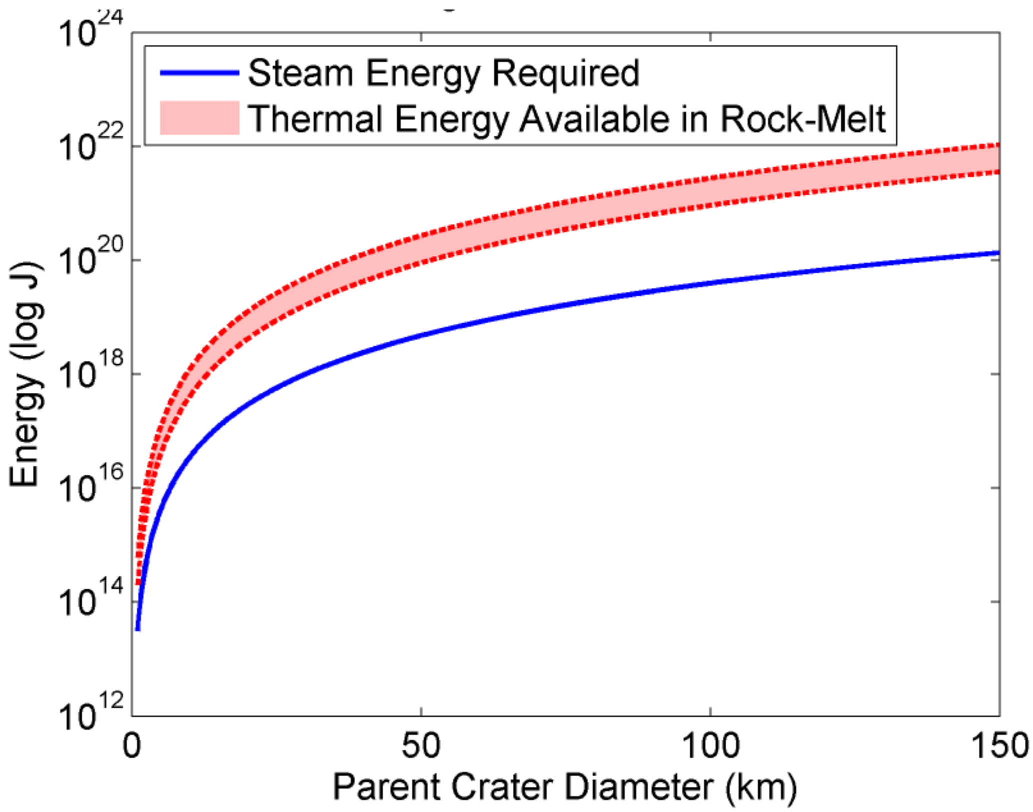

Fig. 12: Thermal energies of water required to convert ice to steam to provide the energy for creating central pit craters (blue line) of differing diameter. Also shown is the available thermal energy from impact melt, after applying thermal efficiency values of 0.1 (lower red curve) to 0.3 (upper red curve).

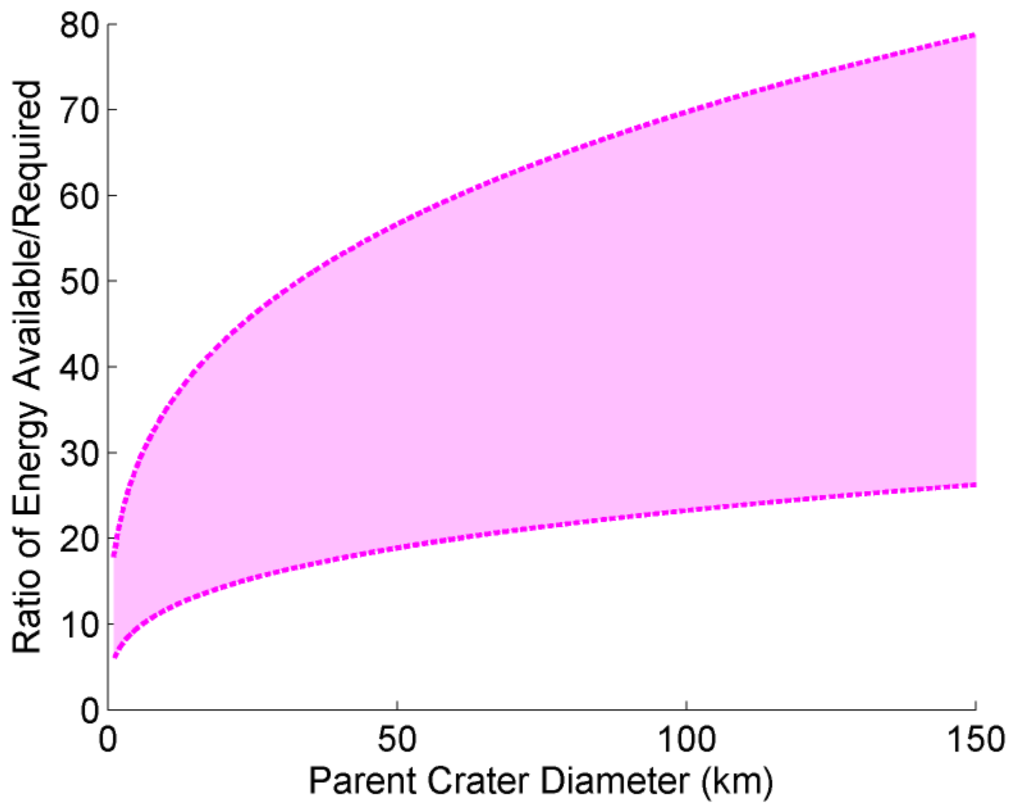

Fig. 13: Ratios of available / required thermal energy for vaporizing enough steam to explode and form a central pit, with respect to crater diameter. The range of in energy ratios reflects variations in heat transfer efficiency over a range of 0.1 (lower curve) to 0.3 (upper curve).

First, an appropriate volume of water must be available in the central uplift. If too little water (or too low a concentration) is present, there may not be sufficient steam to form a large pit. Even if water was initially present in the target rocks, large impacts (with crater diameters of several tens to hundreds of km) likely remove most subsurface volatiles early in the impact process such that not enough water is available to react with the impact melt to form a pit. Conversely, if the system has excess water, there may not be enough thermal energy in the impact melt to heat the excess water and still vaporize enough to sustain an explosion and make a pit.

Second, an appropriate volume of impact melt must be retained within the parent impact crater. Smaller impact craters produce less melt proportionally and distribute that impact melt more sparsely, so small craters may not have enough consolidated impact melt even if enough water is present. Larger impact craters might also produce excess impact melt that could fill in any central pits that might form. A similar phenomenon is thought to have occurred at the Sudbury impact structure, where steam explosions created the brecciated Onaping Formation but the explosive depressions themselves were filled in and erased [Grieve *et al.*, 2010].Another interesting aspect of the uplift contact model is that since our calculations show it only requires small amounts of water (perhaps as little as 2-6% by volume), it provides a possible explanation for the formation of the small number of central pits observed on Mercury [Schultz, 1988; Xiao and Komatsu, 2013] and the Moon [Croft, 1981; Schultz, 1976a, 1976b, 1988; Xiao *et al*., 2014], which should have insufficient water or other volatiles to form by drainage and collapse models [*e.g.* Croft, 1981]. Although we did not measure summit pit-related thermal inertias in our survey, summit pits would be expected to form as in our uplift contact model when steam explosions start but become water- or impact melt-limited. In such a case, the explosive reaction fails before uplift has ceased and an incomplete pit is left superposed on a remnant central peak.

Based on our uplift contact model, we propose the following testable predictions. First, a the ejecta deposit is expected to contain abundant fractured and fragmented glassy impact melt, similar to the Onaping Formation at Sudbury [Grieve *et al*., 2010]. This layer of glassy deposits should overlay more coherent impact melt deposits. Second, lithic clasts and mineral assemblages found stratigraphically below the transient crater should be found on the floor of the parent crater, with the greatest abundance proximal to the rim. Third, the stratigraphic sequence of rocks around central pits should be overturned. Finally, *in situ* measurements of material around the pit should show decreasing average grain sizes with radial distance from central pits.

Conclusions:

The presence of raised rims and blocky material surrounding Martian central pits are suggestive of ejecta from an explosive pit origin. Over 60% of all central pits in our global survey have material with radially decreasing thermal inertias around them, and 89% of central pits craters with diameters >20 km and non-dusty proximal thermal inertias >300 TIU have radially decreasing thermal inertias. The population of central pit craters as a whole has a statistically significant ($P<0.01$) decrease in thermal inertia radially outwards from pit rims. We interpret these findings as a typical decrease in average grain size with increasing distance away from central pits. As expected, dust masks the diurnal thermal signature around many central pits. This effect is amplified in smaller pits due to their less voluminous and finer-grained ejecta that are more easily buried or eroded. Previously proposed models do not satisfactorily explain all observed characteristics of central pits. We have therefore proposed a new "uplift contact model" to explain the observed morphologies (i.e., geometries, raised rims) and thermal properties (radially decreasing thermal inertias/average grain size) of Martian central pit craters. Our thermal calculations show that only ≥ 2-6% water by volume is required to create a phreatomagmatic explosion and form central pits. Our explosive origin model is also advantageous over drainage and collapse models in explaining the small number of central pits on Mercury and the Moon using only minor amounts of volatiles in localized pre-impact subsurfaces. Drainage and collapse may still be a viable method for pit formation on icy satellites, but an explosive origin appears to be the preferred mechanism on Mars (and other rocky planets) for forming central pit craters.

Acknowledgements:

We gratefully acknowledge Robin Fergason for her work on the THEMIS thermal inertia mosaic, JMARS development team, and the THEMIS, CTX, and HiRISE teams. We would also like to extend a special thank you to Devon Burr and Nadine Barlow for their invaluable time in reviewing and improving this manuscript.

References:

Alzate, N., Barlow, N.G., 2011. Central pit craters on Ganymede. Icarus 211, 1274-1283.

Baloga, S.M., Fagents, S.A., Mouginis-Mark, P.J., 2005. Emplacement of Martian Rampart Crater Deposits. J. Geophys. Res. 110, E10001. doi:10.1029/2004JE002338.

Barlow, N.G., 2006. Impact Craters in the Northern Hemisphere of Mars: Layered Ejecta and Central Pit Characteristics. Met. & Planet. Sci. 41, 1425-1436.

Barlow, N.G., 2010. Central pit craters: Observations from Mars and Ganymede and implications for formation models. GSA Special Papers 465, 15-27.

Barlow, N.G., 2011. Constraints on the Proposed Formation Models for Martian Central Pit Craters. Lunar Planet. Sci. 42. Abstract #1149.

Barlow, N. G., Bradley, T. L., 1990. Martian impact craters: Correlations of ejecta and interior morphologies with diameter, latitude, and terrain. Icarus, 87(1), 156-179.

Barlow, N.G., Boyce, J.M., Costard, F.M., Craddock, R.A., Garvin, J.B., Sakimoto, S.E.H., Kuzmin, R.O., Roddy, D.J., 2000. Standardizing the Nomenclature of Martian Impact Crater Ejecta Morphologies. J. Geophys. Res. 105, E11, 26733-26738.

Begét, J.E., Hopkins, D.M., Charron, S.D., 1996. The Largest Known Maars on Earth, Seward Peninsula, Northwest Alaska. Arctic 49, 1, 62-69.

Bell, J.F., III, Malin, M.C., Caplinger, M.A., Fahle, J., Wolff, M.J., Cantor, B.A., James, P.B., Ghaemi, T., Posiolova, L.V., Ravine, M.A., Supulver, K.D., Calvin, W.M., Clancy, R.T., Edgett, K.S., Edwards, L.J., Haberle, R.M., Hale, A., Lee, S.W., Rice, M.S., Thomas, P.C., Williams, R.M.E., 2013. Calibration and Performance of the Mars Reconnaissance Orbiter Context Camera (CTX). Mars 8, 1-14. doi:10.1555/mars.2013.0001.

Boyce, J. M., Wilson, L., Mouginis-Mark, P. J., Hamilton, C. W., Tornabene, L. L., 2012. Origin of small pits in martian impact craters. Icarus, 221(1), 262-275.

Boynton, W.V., Taylor, G.J., Evans, L.G., Reedy, R.C., Starr, R., Janes, D.M., Kerry, K.E., Drake, D.M., Kim, K.J., Williams, R.M.S., Crombie, M.K., Dohm, J.M., Baker, V., Metzger, A.E., Karunatillake, S., Keller, J.M., Newsom, H.E., Arnold, J.R., Bruckner, J., Englert, P.A.J., Gasnault, O., Sprague, A.L., Mitrofanov, I., Squyres, S.W., Trombka, J.I., d'Uston, L., Wanke, H., Hamara, D.K., 2007. Concentration of H, Si, Cl, K, Fe, and Th in the low- and mid-latitude regions of Mars. J. Geophys. Res. 112, E12S99. doi:10.1029/2007JE002887.

Bray, V. J., 2009. Impact crater formation on the icy Galilean satellites. Doctoral dissertation, Imperial College London.

Bray, V.J., Schenk, P.M., Melosh, H.J., Morgan, J.V., Collins, G.S., 2012. Ganymede crater dimensions – Implications for central peak and central pit formation and development. Icarus 217, 115-129.

Buhl, E., Sommer, F., Poelchau, M.H., Dresen, G., Kenkmann, T., 2014. Ejecta from experimental impact craters: Particle size distribution and fragmentation energy. Icarus 237, 131-142.

Carr, M.H., Crumpler, L.S., Cutts, J.A., Greeley, R., Guest, J.E., Masursky, H., 1977. Martian Impact Craters and Emplacement of Ejecta by Surface Flow. J. Geophys. Res. 82, 28, 4055-4065.

Caudill, C. M., Tornabene, L. L., McEwen, A. S., Byrne, S., Ojha, L., & Mattson, S., 2012. Layered MegaBlocks in the central uplifts of impact craters. Icarus, 221(2), 710-720.

Christensen, P.R., 1986. The Spatial Distribution of Rocks on Mars. Icarus 68, 217-238.

Christensen, P.R., Bandfield, J.L., Hamilton, V.E., Ruff, S.W., Kieffer, H.H., Titus, T.N., Malin, M.C., Morris, R.V., Lane, M.D., Clark, R.L., Jakosky, B.M., Mellon, M.T., Pearl, J.C., Conrath, B.J., Smith, M.D., Clancy, R.T., Kuzmin, R.O., Roush, T., Mehall, G.L., Gorelick, N., Bender, K., Murray, K., Dason, S., Greene, E., Silverman, S., Greenfield, M., 2001. Mars Global Surveyor Thermal Emission Spectrometer experiment: Investigation description and surface science results. J. Geophys. Res. 106, E10, 23823–23871.

Christensen, P.R., Engle, E., Anwar, S., Dickenshied, S., Noss, D., Gorelick, N., Weiss-Malik, M., 2009. JMARS – A Planetary GIS. http://adsabs.harvard.edu/abs/2009AGUFMIN22A..06C.

Christensen, P.R., Jakosky, B.M., Kieffer, H.H., Malin, M.C., McSween, H.Y., Jr., Nealson, K., Mehall, G.L., Silverman, S.H., Ferry, S., Caplinger, M., Ravine, M., 2004. The Thermal Emission Imaging System (THEMIS) for the Mars 2001 Odyssey Mission. Space Sci. Rev. 110, 85-130.

Clifford, S.M., Hillel, D., 1983. The Stability of Ground ice in the Equatorial Region of Mars. J. Geophys. Res. 88, B3, 2456-2474.

Croft, S.K., 1981. On the Origin of Pit Craters. Proc. Lunar Planet. Sci. Conf. 12, 196-198.

Cushing, G.E., Titus, T.N., Wynne, J.J., Christensen, P.R., 2007. THEMIS observes possible cave skylights on Mars. Geophys. Res. Let. 34, L17201. doi:10.1029/2007GL030709.

Edwards, C.S., Bandfield, J.L., Christensen, P.R., Fergason, R.L., 2009. Global Distribution of Bedrock Exposures on Mars using THEMIS High-resolution Thermal Inertia. J. Geophys. Res. 114, E11001. doi:10.1029/2009JE003363.

Edwards, C.S., Nowicki, K.J., Christensen, P.R., Hill, J., Gorelick, N., Murray, K., 2011. Mosaicking of global planetary image datasets: 1. Techniques and data processing for Thermal Emission Imaging System (THEMIS) multi-spectral data. J. Geophys. Res. 116, E10008. doi:10.1029/2010JE003755.

Elder, C.M., Bray, V.J., Melosh, H.J., 2012. Theoretical Plausibility of Central Pit Crater Formation Via Melt Drainage. Icarus 221, 831-843.

Fergason, R.L., Christensen, P.R., Kieffer, H.H., 2006. High Resolution Thermal Inertia Derived from THEMIS: Thermal Model and Applications. J. Geophys. Res. 111, E12004. doi:10.1029/2006JE002735.

French, B.M., 1998. Traces of Catastrophe. LPI Contribution No. 954, Lunar and Planet. Inst., Houston, Texas.

Garner, K. M. L., Barlow, N. G., 2012. Distribution of rimmed, partially rimmed, and non-rimmed central floor pits on Mars. LPSC 43, Abstract #1256.

Garvin, J. B., Sakimoto, S. E., Frawley, J. J., 2000. Craters on Mars: Global Geometric Properties from Gridded MOLA topography. Mars 5, Abstract #3277.

Garvin, J. B., Sakimoto, S. E., Frawley, J. J., Schnetzler, C. 2000. North polar region craterforms on Mars: Geometric characteristics from the Mars Orbiter Laser Altimeter. Icarus, 144(2), 329-352.

Gault, D.E., Greeley, R., 1978. Exploratory Experiments of Impact Craters Formed in Viscous-Liquid Targets: Analogs for Martian Rampart Craters?. Icarus 34, 486-495.

Gault, D.E., Shoemaker, E.M., Moore, H.J., 1963. Spray Ejected from the Lunar Surface by Meteoroid Impact. NASA Technical Note D-1767.

Greeley, R., Fink, J.H., Gault, D.E., Guest, J.E., 1982. Experimental simulation of impact cratering on icy satellites. In D. Morrison (Ed.), Satellites of Jupiter. University of Arizona Press, Tucson, Arizona. pp. 340-378.

Grieve, R.A.F., Ames, D.E., Morgan, J.V., Artemieva, N., 2010. The evolution of the Onaping Formation at the Sudbury impact structure. Met. Planet. Sci. 45, 5, 759-782.

Head, J. W., Mustard, J.F., Kreslavsky, M.A., Milliken, R.E., Marchant, D.R., 2003. Recent Ice Ages on Mars. Nature 426, 797-802.

Hodges, C.A., 1978. Central Pit Craters on Mars. Proc. Lunar Planet. Sci. Conf. 9, 521-522.

Hodges, C.A., Shew, N.B., Clow, G., 1980. Distribution of Central Pit Craters on Mars. Proc. Lunar Planet. Sci. Conf. 11, 450-452.

Ivanov, B. A., Neukum, G., Bottke, W. F., & Hartmann, W. K., 2002. The comparison of size-frequency distributions of impact craters and asteroids and the planetary cratering rate.

Asteroids III, 1, 89-101.Judd, W. R., Shakoor, A., 1989. Density in Physical Properties of Rocks and Minerals (ed. C. Y. Ho et al.), Philadelphia, PA: Taylor and Francis, pp. 409–502.

Malin, M.C., Bell, J.F., III, Cantor, B.A., Caplinger, M.A., Calvin, W.M., Clancy, R.T., Edgett, K.S., Edwards, L., Haberle, R.M., James, P.B., Lee, S.W., Ravine, M.A., Thomas, P.C., Wolff, M.J., 2007. Context Camera Investigation on board the Mars Reconnaissance Orbiter. J. Geophys. Res. 112, E05S04. doi:10.1029/2006JE002808.

McEwen, A.S., Eliason, E.M., Bergstrom, J.W., Bridges, N.T., Hansen, C.J., Delamere, W.A., Grant, J.A., Gulick, V.C., Herkenhoff, K.E., Keszthelyi, L., Kirk, R.L., Mellon, M.T., Squyres, S.W., Thomas, N., Weitz, C.M., 2007. Mars Reconnaissance Orbiter's High Resolution Imaging Science Experiment (HiRISE). J. Geophys. Res. 112, E05S02. doi:10.1029/2005JE002605.

McEwen, A.S., Preblich, B.S., Turtle, E.P., Artemieva, N.A., Golombek, M.P., Hurst, M., Kirk, R.L., Burr, D.M., Christensen, P.R., 2005. The rayed crater Zunil and interpretations of small impact craters on Mars. Icarus 176, 351-381.

Mellon, M.T., Jakosky, B.M., Postawko, S.E., 1997. The Persistence of Equatorial Ground Ice on Mars. J. Geophys. Res. 102, E8, 19357-19369.

Melosh, H.J., 1989. Impact Cratering: A Geologic Process. Oxford Monographs on Geology and Geophysics #11, Oxford University Press, New York.

Moran, M. J., Shapiro, H. N., Boettner, D. D., & Bailey, M., 2010. Fundamentals of Engineering Thermodynamics. John Wiley & Sons.

O'Keefe, J. D., & Ahrens, T. J., 1982. Cometary and meteorite swarm impact on planetary surfaces. J. Geophys. Res. 87(B8), 6668-6680.

O'Keefe, J.D., Ahrens, T.J., 1985. Impact and Explosion Crater Ejecta, Fragment Size, and Velocity. Icarus 62, 328-338.

Okubo, C.H., Martel, S.J., 1998. Pit crater formation on Kilauea volcano, Hawaii. J. Volc. Geothermal Res. 86, 1-18.

Passey, Q.R., Shoemaker, E.M., 1982. Craters and basins on Ganymede and Callisto: Morphological indicators of crustal evolution. In: Morrison, D. (Ed.), Satellites of Jupiter. Univ. of Arizona Press, Tucson, Arizona. pp. 379-434.

Robinson, M.S., Ashley, J.W., Boyd, A.K., Wagner, R.V., Speyerer, E.J., Hawke, B.R., Hiesinger, H., van der Bogert, C.H., 2012. Confirmation of sublunarean voids and thin layering in mare deposits. Planet. Space Sci. 69, 18-27.

Salvati, R., Sasowsky, I.D., 2002. Development of collapse sinkholes in areas of groundwater discharge. J. Hydrology 264, 1-11.

Sato, H., Taniguchi, H., 1997. Relationship Between Crater Size and Eject Volume of Recent Magmatic and Phreato-magmatic Eruptions: Implications for Energy Partitioning. Geophys. Res. Let. 24, 3, 205-208.

Schultz, P.H., 1976a. Floor-fractured lunar craters. Moon 15, 241-273.

Schultz, P.H., 1976b. Moon Morphology. University of Texas Press, Austin, Texas.

Schultz, P.H., 1988. Cratering on Mercury: A Relook. In: Villas, F., Chapman, C.R., Matthews, M.S. (Eds.), Mercury, University of Arizona Press, Tucson, Arizona, pp. 274-335.

Segura, T. L., Toon, O. B., Colaprete, A., & Zahnle, K., 2002. Environmental effects of large impacts on Mars. Science, 298(5600), 1977-1980.

Smith, E.I., 1976. Comparison of the Crater Morphology-Size Relationship for Mars, Moon, and Mercury. Icarus 28, 543-550.

Smith, B.A., Soderblom, L.A., Beebe, R., Boyce, J., Briggs, G., Carr, M., Collins, S.A., Cook, A.F., II, Danielson, G.E., Davies, M.E., Hunt, G.E., Ingersoll, A., Johnson, T.V., Masursky, H., McCauley, J., Morison, D., Owen, T., Sagan, C., Shoemaker, E.M., Strom, R., Suomi, V., Veverka, J., 1979. The Galilean Satellites and Jupiter: Voyager 2 Imaging Science Results. Science 206, 927-950.

Smith, D.E., Zuber, M.T., Frey, H.V., Garvin, J.B., Head, J.W., Muhleman, D.O., Pettengill, G.H., Phillips, R.J., Solomon, S.C., Zwally, H.J., Banerdt, W.B., Duxbury, T.C., Golombek, M.P., Lemoine, F.G., Newmann, G.A., Rowlands, D.D., Aharonson, O., Ford, P.G., Ivanov, A.B., Johnson, C.L., McGovern, P.J., Abshire, J.B., Afzal, R.S., Sun, X. 2001. Mars Orbiter Laser Altimeter: Experiment Summary After the First Year of Global Mapping of Mars. J. Geophys. Res. 106, E10, 23689-23722.

Tornabene, L. L., Ling, V., Osinski, G. R., Boyce, J. M., Harrison, T. N., & McEwen, A. S., 2013. A Revised Global Depth-Diameter Scaling Relationship for Mars Based on Pitted Impact Melt-Bearing Craters. LPSC 44, Abstract #2592.

Tornabene, L.L., Moersch, J.E., McSween, H.Y., Jr., McEwen, A.S., Piatek, J.L., Milam, K.A., Christensen, P.R., 2006. Identification of large (2-10) km rayed craters on Mars in THEMIS thermal infrared images: Implications for possible Martian meteorite source regions. J. Geophys. Res. 111, E10006. doi:10.1029/2005JE002600.

Tornabene, L. L., Osinski, G. R., McEwen, A. S., Boyce, J. M., Bray, V. J., Caudill, C. M., ... & Mouginis-Mark, P. J., 2012. Widespread crater-related pitted materials on Mars: Further evidence for the role of target volatiles during the impact process. Icarus, 220(2), 348-368.

Xiao, Z., Komatsu, G., 2013. Impact craters with ejecta flows and central pits on Mercury. Plan. Space Sci.. doi:10.1016/j.pss.2013.03.015.

Xiao, Z., Zeng, Z., Komatsu, G., 2014. A global inventory of central pit craters on the Moon: Distribution, morphology, and geometry. Icarus 227, 195-201.

White, J.D.L., Ross, P.-S., 2011. Maar-Diatreme Volcanoes: A Review. J. Volc. Geotherm. Res. 201, 1-29.

Wohletz, K. H., 1986. Explosive Magma-water Interactions: Thermodynamics, Explosion Mechanics, and Field Studies. Bull. Volc. 48, 245-264.

Wohletz, K.H., Sheridan, M.F., 1983. Martian Rampart Crater Ejecta: Experiments and Analysis of Melt-Water Interaction. Icarus 56, 15-37.

Wood, C.A., Head, J.W., Cintala M.J., 1978. Interior Morphology of Fresh Martian Craters: The Effects of Target Characteristics. Proc. Lunar Planet. Sci. Conf. 9, 3691-3709.

Zieg, M. J., & Marsh, B. D., 2005. The Sudbury Igneous Complex: Viscous emulsion differentiation of a superheated impact melt sheet. Geological Society of America Bulletin, 117(11-12), 1427-1450.